Processes and rates of formation defined by modelling in alkaline to acidic soil systems in Brazilian Pantanal wetland

Patricia Merdy, Mohamed Gamrani, Célia R Montes, Ary Rezende Filho, Laurent Barbiero, Débora A Ishida, André R.C. Silva, Adolpho Melfi, Yves Lucas

Catena, 2023, (222), 106837

[DOI: 10.1016/j.catena.2022.106837]

Processes and rates of formation defined by modelling in alkaline to acidic soil systems in Brazilian Pantanal wetland

Patricia Merdy[a*], Mohamed Gamrani[a], Célia R. Montes[b,e], Ary T. Rezende Filho[c], Laurent Barbiero[d], Débora A. Ishida[e], André R.C. Silva[b], Adolpho J. Melfi[e], Yves Lucas[a]

[a] *Université de Toulon, Aix Marseille Université, CNRS, IM2NP, 83041 Toulon CEDEX 9, France*
[b] *CENA, NUPEGEL, Universidade de São Paulo, Piracicaba 13400-970, Brazil*
[c] *FAENG, Universidade Federal do Mato Grosso do Sul, Campo Grande 79079-900, Brazil*
[d] *GET, IRD, CNRS, UPS, OMP Toulouse 31400, France*
[e] *IEE, NUPEGEL, Universidade de São Paulo, São Paulo 05508-010, Brazil*

*Corresponding author (merdy@univ-tln.fr)

Keywords :

Soil formation rate
PHREEQC model
Saline and alkaline soils
Soil pH change
Wetlands

ABSTRACT

Within a soil system, it is generally difficult to relate the observed secondary phases and their spatial distribution to past or current processes. Geochemical modelling can help to identify present-days processes and to quantify formation rates if the system is sufficiently constrained. Here we used the PHREEQC model for this purpose, applying it to soil alkaline to acidic soil systems in the Nhecolândia area. A large amount of data was available, but scientific questions remained opened. We carried out a complementary field study to clarify a key point necessary for modelling, confirming the disconnection between two types of groundwater, perched, alkaline and deep, acidic. Our simulations showed that the observed soil system corresponds to the current biogeochemistry and that paleoclimatic genetic hypotheses are unnecessary. We found that the ridge soil formation rate ranges from 396 to 638 kg ha^{-1} y^{-1}, depending on hypotheses. We showed that the downslope soils act as buffers to store labile species during the dry season, allowing alkalinity to be maintained from one year to the next. At least 125 y were necessary to obtain downslope alkaline lakes, and this alkaline nature can quickly disappear after changing drainage conditions. We explained how hyperacidic horizons (pH<4) can neighbor alkaline horizons (pH>10) with a sharp contact. When correctly informed, geochemical modelling appeared as an effective tool to answer questions about soil processes.

1. Introduction

Pedological processes accompany changes in pedoclimatic conditions of various origins. They tend to bring the soil into a state in which its mineral constituents are in equilibrium with the soil solutions. Most often, these processes are slow, so that the soil can be a recorder of past environmental conditions, which is frequently used for the reconstruction of paleoenvironments. Some reactions, however, are rapid, particularly when they involve circulations of soluble salts, changes in redox conditions, and associated processes. Under certain favorable conditions, dating of secondary phases makes it possible to estimate the speed of these changes (Barbiero et al., 2010; Schmidt et al., 2015; Mathian et al., 2019). Such conditions are difficult to meet, and the use of geochemical modeling coupled to mass balance along a slope (Yoo et al., 2007) or on small watersheds (Huang et al., 2013) may allow the estimation of weathering or soil formation rates. Geochemical modelling is also a way to identify possible present-day processes and to estimate formation rates (Lecomte et al., 2005). However, such studies are scarce, likely because they require in-depth knowledge of the mineralogy and the hydro-geochemistry of the studied system to constrain it sufficiently.

Such knowledge is available for the Lower Nhecolândia soils (Fig. 1), a subregion of the Pantanal huge wetland in Brazil, which drew attention due to the presence of many small lakes with very contrasting water chemistry, from fresh to highly alkaline water: for two adjacent lakes separated by less than 200 m, one can have pH<6 and the other, a pH>10. Strong contrasts have also been observed for the surrounding soils, where horizons of pH> 10 can be found within a few 10 centimeters of horizons with a pH of 3.5 (Barbiero et al., 2008). The fundamental question posed is the origin of such contrasts when the whole system is developed on the same sandy sediment. Moreover, the negative annual hydric balance between rainfall and evapotranspiration (Alho, 2008) can only insufficiently explain the observed alkalinity.

In this sense, the Nhecolândia lakes and their surrounding soil systems have been the subject of numerous studies over the last 20 years, with the aim to reconstitute the paleoenvironments, or

more generally the environmental conditions, that have given rise to such ecologically contrasted landscape units. These studies, summarised below, have given well-argued hypotheses on the genesis of the system, pointing out the role of soil water hydrodynamics and lateral flows in semi-arid regions pedogenesis. They, however, left open questions such as the system formation time with regard to paleoclimatic variations, the relationships between regional, acidic, and local, alkaline water tables and the processes that result in the juxtaposition of horizons with a pH difference greater than 10. These studies provide sufficient quantitative data to run the PHREEQC model (Parkhurst and Appelo, 2013) to confirm, or invalidate, the key hypotheses of the geochemistry of the soil system. This model has already been used on Pantanal soil solutions, but only to assess the saturation of the solutions with respect to the minerals observed (Barbiero et al., 2008), while the model allows direct or inverse modeling of the composition of the soil solution between two locations of the soil cover.

In this context, the aim of this work is twofold. On the one hand, we carried out field observations in order to confirm the geographical range of the processes, and to clarify the relationships between the regional water table and the alkaline water table surrounding the alkaline lakes, which is a prerequisite for defining the models. On the other hand, we ran the PHREEQC models, feeding it with the extensive input data on lake and groundwater chemistry and soil mineralogy, existing or acquired in this study. The goal was to reproduce the reactions occurring between the different compartments (minerals, rainwater, groundwater and lake water), to check their feasibility, and to establish a mass balance at the scale of this soil system.

2. Site context and background results

The Pantanal area, recognised as the largest wetland of the world, is an active, subsiding sedimentary basin that began to form at least 15 My ago. The basin infill consists of coarse- to fine-grained sandstones and unconsolidated sediments with little diagenesis. No relationship was found between the type of lake and the nature of the underlying sediment (Assine et al., 2015). Most of the Pantanal is subjected to a seasonal flooding that approximatively lasts from January to June with a large interannual variability (Marengo et al., 2015). Within the Pantanal, the Lower Nhecolândia is characterised by around 9000 shallow lakes, mostly ranging from 0.025 to 0.15 km^2 (Costa et al., 2015). Most are freshwater lakes connected to the surface drainage network, but around 7 % are unconnected, alkaline water lakes (Pereira et al., 2020) ranging from brackish to saline (Furian et al., 2013, Furquim et al., 2017). Vegetation is a savanna forest (cerrado) on ridges and a succession of savanna woodland, open woody savanna, open shrubby grassland and savanna grassland on the slopes from ridges to lakes or channels (Salis et al., 2014). Annual precipitation and potential evaporation in this region are, on average, 1,100 and 1,400 mm, respectively, resulting in a negative hydric balance (Alho, 2008). However, this is insufficient to simply explain the occurrence of such alkaline lakes. Rainfall exceeds potential evapotranspiration from November to March for a total of about 210 mm (Hamilton et al., 1998) which is sufficient to leach out soluble species that may accumulate in soils during periods of water deficit. The processes identified in humid zones of more arid zones, such as the concentration of salt in groundwater by the absorption of water by the roots of trees in the Okavango delta islands (McCarthy and Ellery, 1994), do not take place here.

Data compiled from various sources and locations (Barbiero et al., 2002; Furian et al., 2013; Costa et al., 2015; Guerreiro et al., 2019) (Fig. 1) that are consistent with each other show that the freshwater lakes have values of pH, electric conductivity and total dissolved solids (TDS) of around 6.5, 130 µS cm^{-1} and 110 ppm, respectively, whereas for alkaline lakes these parameters are mainly in the range of 9.4–9.8, 1,400–1,800 µS cm^{-1} and 1,300–2,100 ppm, respectively. Some alkaline lakes exhibit a green colour due to cyanobacterial blooms, whereas others exhibit a black colour due to dissolved organic matter, without the occurrence of cyanobacterial bloom (Andreote et al, 2014;

Barbiero et al., 2018). The geochemical type of a given lake most often remains the same from one year to the next, although it can change after an unusually rainy or dry season (Bergier et al., 2014).

As early as 2002, it was established that the waters of the different types of lakes and the groundwater of the surrounding soils could all derive from the floodwaters and that it was not necessary to assume a salinity inherited from alternating arid and humid phases dating from the Pleistocene (Barbiero et al., 2002). This hypothesis was later reinforced by isotopic measurements (Almeida et al., 2010). In 2008, it was shown that the current water regime of alkaline lakes is one-way, from surrounding surfaces to alkaline lakes, which qualitatively explains salinity as a result of ongoing processes. Conversely, freshwater lakes are crossed each year by water circulating regionally, which helps to maintain the low salinity (Barbiero et al., 2008). There is therefore a close relationship between the soils surrounding the lakes, the hydrodynamics of subsurface waters and the lake chemistry. The formation of greenish horizons, (green sandy loam), with a low hydraulic conductivity, results in hydrological thresholds that control the groundwater fluxes between a saline-alkaline area and the surroundings.

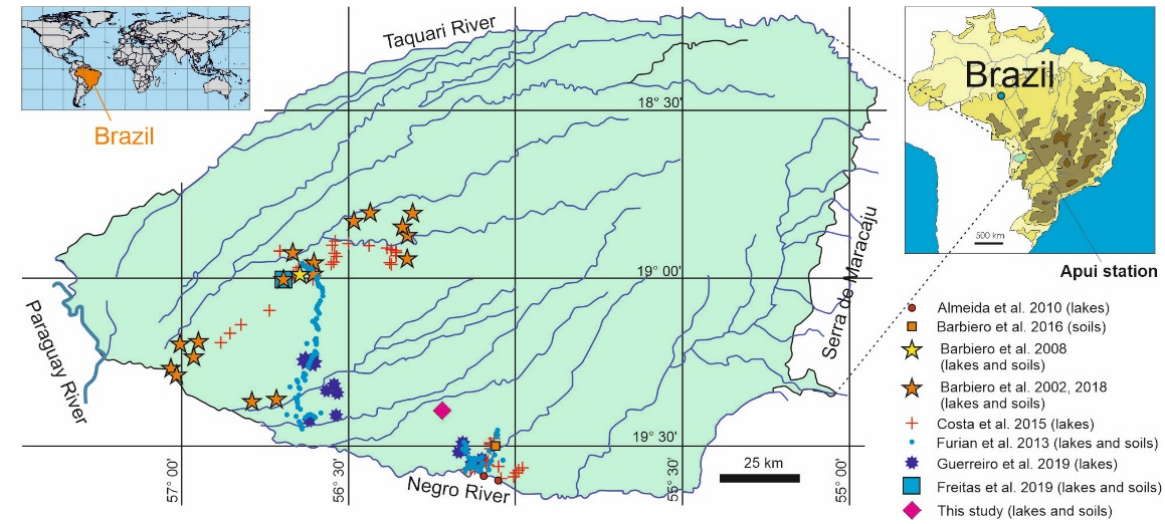

Fig. 1. The Nhecolândia area and location of the present study and studies whose data have been used or cited.

The hypothesised seasonal dynamics of an alkaline lake and the structure of the surrounding soils proposed in Barbiero et al. (2008) was confirmed by several other studies carried out at other sites, a synthesis of which was proposed by Furian et al. (2013). These results are summarized in Fig. 2. During the dry season, the lake water evaporates both by its free surface and by the downslope topsoil, where it is transferred by capillarity. This results in the precipitation of amorphous silica, Ca- and Mg minerals close to the lake shore (Furquim et al. 2008, 2010b) and K-minerals a few meters away (Furquim et al. 2010a; Barbiero et al. 2016), while the soil solution reaches almost equilibrium with respect to Na-carbonate (Barbiero et al., 2002). The paragenesis observed here (Ca and Mg carbonates, Mg-smectites, Fe-illites and mixed-layered phyllosilicates, amorphous silica) were already mentioned for areas where evaporation controls mineral neoformations in alkaline conditions, such as the Chad Lake, the Niger inland delta in Mali or the Okavango delta (Maglione, 1974; Valles et al., 1989; McCarty and Metcalfe, 1990). The potential equilibrium of these minerals with present-days geochemistry of the groundwaters was assessed by thermodynamic calculation (Barbiero et al., 2002; 2008).

The deep groundwater can rise by capillarity in the ridge, where a 10-cm-thick silcrete can sometimes be observed, around 2 m in depth. At the lower part of the slopes, however, the low hydraulic conductivity of the green sandy loam horizons prevents both the lake alkaline water to percolate in depth and deep, fresh groundwater to rise into the lake: during most of the year there is a disconnection between the aquifers perched over the green sandy loam and the deep aquifer.

During the wet season, the aquifers reconnect. The deep water table rises and the fresh groundwater overflows the green horizon threshold and laterally percolates towards the lake through the horizons located above the green sandy loam , dissolving minerals that had precipitated during the dry season (Fig. 2). The rainwater which infiltrates the slopes participates in this process. As a result, the water that arrives at the lake is already more alkaline than the fresh groundwater. Freitas et al. (2019), however, did not consider disconnection between aquifers during the dry season and assumed that alkaline lakes do not receive groundwater inflow and act as a recharge zone. The question of the relationships between the alkaline lake water and the deep groundwater remains therefore open.

3. Material and methods

3.1. Study site and field work

Soils were studied during the dry season along a toposequence situated in the São Roque farm, at 19° 22' 53'' S, 56° 19' 42'' W, on the slope of an alkaline lake beach. Boreholes made with a manual auger were cased during drilling with ABS tubes (Eijkelkamp) to prevent the soil from collapsing and the solutions from different waterlogged horizons from mixing.

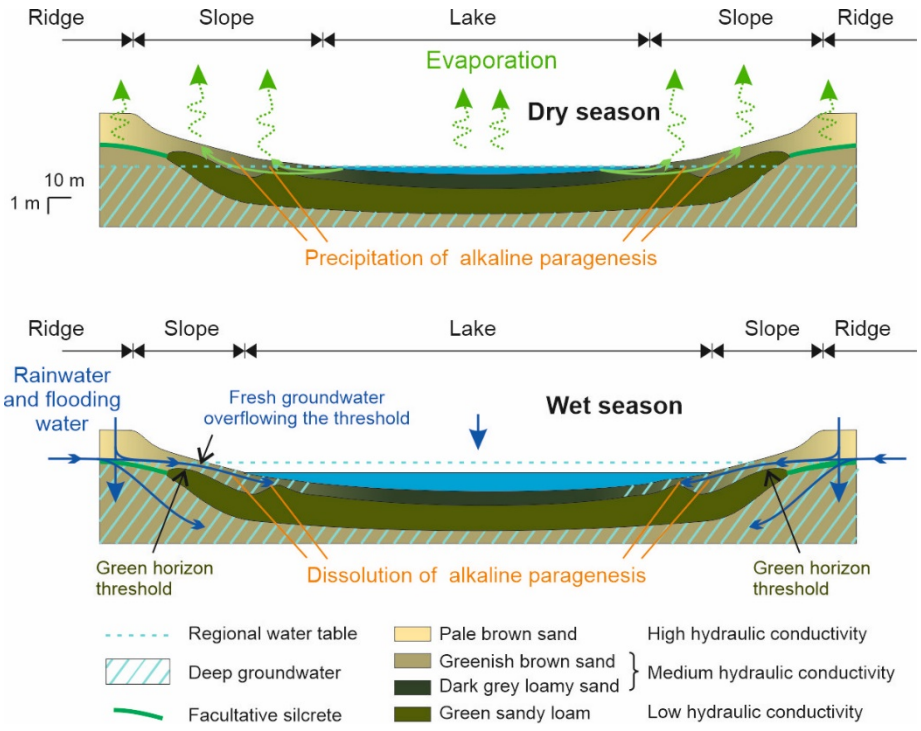

Fig. 2. Seasonal dynamics of an alkaline lake related to water fluxes and main horizons.

In these horizons, the soil water was sampled with a sampling rod at a given depth during drilling, which ensured that the water was coming from the depth reached by drilling. Water pH and conductivity were immediately measured in the field, in order to avoid a modification of these parameters due to the exchange of O_2 or CO_2 with the atmosphere. The water table depths were determined from the appearance of free water in the auger sampling at the time of drilling; the casing tube was left in place and the water table depth was measured 24 h later. In the case of a borehole where two water tables were separated by horizons in which no free water could be

perceived (green sandy loam), the depth of the deep water table was determined first at the time of drilling by the reappearance of free water in the auger sampling, then after 24 h in the casing tube left in place. A rise in the water table indicates that it was confined under pressure below a horizon with low permeability. The characteristics of the sandy loam ensured a good sealing along the casing tube. The effectiveness of the sealing was checked during drilling – no water must enter the casing tube when drilling through the green sandy loam – and by a simple pH measurement after rising of the deep water table. The pH of the deep water table is less than 7 when that of the water table perched over the green sandy loam is usually higher than 8.5. We measured in the borehole the pH of the deep water when it was reached during drilling before it rose, then after it rose. Obtaining the same pH guaranteed that the water risen in the borehole actually came from the deep water table.

The soil samples were air-dried and aliquots were separated for particle-size and mineralogical characterisation; it should be noted that drying is likely to transform reactive reduced minerals, such as fougerite (Feder et al., 2018), or to precipitate evaporitic minerals. A detailed description of the soil sequence will be the subject of a future paper; here, we used the only data necessary to perform the modelling.

3.2. Data from the literature

3.2.1. Soil and alkaline lake water

The water chemistry values of soil and alkaline lakes used for modelling are the same as those used in the work of Barbiero et al. (2008), in which the methods of sampling and analysis were described. Regarding soil and alkaline lake solutions, we used a set of data issued from the same location to ensure consistency among the data; the values we used are given in Table 1. Most values are the average of more than 10 measurements. The alkaline lake values are in the range of the values given in other studies (Barbiero et al., 2002; Furian et al., 2013; Bergier et al., 2014; Costa et al., 2015).

3.2.2. Rainfall and flooding water

The chemistry of rainfall was not available for the Pantanal, and therefore, we used data from the South Amazonia Apuí station (Honório et al., 2010) (Table 1). Although this station is far from the Pantanal (Fig. 1), it represents a rain in a continental, low elevation area without maritime or Andean influence and the majority of rainfall in the Pantanal originates as water vapor from the Amazon basin (Oliveira et al., 2019).

The flooding water chemistry values correspond to the wet season chemistry of the Taquari River, provided in Rezende Filho et al. (2012). These values are similar to those provided in Oliveira et al. (2019), which correspond to discharge-weighted averages over 7 years. The Fe and Al values, however, lack in the study by Rezende Filho et al. (2012). The Fe value we used was therefore taken from a similar soil system studied by Oliveira et al. (2019) in Northern Pantanal. Data on dissolved Al values in rivers are very scarce. Here we considered an interval of dissolved Al values based on data from U.S. rivers (Förstner, 1981), Zaïre and Niger rivers (Van Bennekom and Jager, 1978) and Turkish rivers (Dundar and Altundag, 2018), and we verified the effect of the change in dissolved Al value on the modeling results.

Table 1
Chemistry of the solutions used in modelling. Data in µS cm^{-1} for electric conductivity (EC), in mol L^{-1} for alkalinity (Alc.) and species. Average value and standard deviation in parentheses when available, n: number of values.

	Rainwater[a]	Alkaline lake water (ALW) n=10	Ridge deep groundwater[b] (DG) n=18	Alkaline deep horizons groundwater[b] (ADHG) n = 23	Hyperacidic groundwater[b] n = 5	Flooding water[c]
pH	5.6	9.6 (0.3)	6.3 (0.8)	8.6 (0.7)	3.8 (0.5)	6.4
EC		$1.2\ 10^{4}$ ($1.02\ 10^{4}$)	$3.9\ 10^{2}$ ($0.3\ 10^{2}$)	$7.6\ 10^{3}$ ($6.4\ 10^{3}$)	$1.2\ 10^{3}$ ($1.1\ 10^{3}$)	$2.3\ 10^{2}$
Alc.	$2.5\ 10^{-6}$	$6.8\ 10^{-2}$ ($3.8\ 10^{-2}$)	$3.7\ 10^{-4}$ ($3.0\ 10^{-4}$)	$5.3\ 10^{-2}$ ($4.4\ 10^{-2}$)	0	$1.1\ 10^{-4}$
F^-	$8.0\ 10^{-6}$	$4.2\ 10^{-4}$ ($2.4\ 10^{-4}$)	< dl	$2.2\ 10^{-4}$ ($2.3\ 10^{-4}$)	$2.0\ 10^{-5}$ ($1.5\ 10^{-5}$)	
Cl^-	$2.8\ 10^{-5}$	$6.7\ 10^{-2}$ ($3.8\ 10^{-2}$)	$8.0\ 10^{-5}$ ($6.7\ 10^{-5}$)	$3.8\ 10^{-2}$ ($3.4\ 10^{-2}$)	$1.9\ 10^{-2}$ ($1.6\ 10^{-2}$)	$2.7\ 10^{-5}$
Br^-		$1.1\ 10^{-4}$ ($0.4\ 10^{-4}$)	< dl	$6.0\ 10^{-5}$ ($6.3\ 10^{-5}$)	$3.0\ 10^{-5}$ ($2.0\ 10^{-5}$)	
SO_4^{2-}	$2.0\ 10^{-5}$	$4.8\ 10^{-4}$ ($2.0\ 10^{-4}$)	$3.0\ 10^{-5}$ ($2.5\ 10^{-5}$)	$7.4\ 10^{-4}$ ($6.7\ 10^{-4}$)	$2.0\ 10^{-6}$ ($1.5\ 10^{-6}$)	$3.9\ 10^{-5}$
Ca^{2+}	$6.0\ 10^{-6}$	$8.1\ 10^{-4}$ ($2.8\ 10^{-4}$)	$6.0\ 10^{-5}$ ($5.8\ 10^{-5}$)	$8.9\ 10^{-4}$ ($8.1\ 10^{-4}$)	$1.6\ 10^{-3}$ ($0.6\ 10^{-3}$)	$6.5\ 10^{-4}$
Mg^{2+}	$4.0\ 10^{-6}$	$1.6\ 10^{-4}$ ($1.1\ 10^{-4}$)	$2.0\ 10^{-5}$ ($2.0\ 10^{-5}$)	$4.4\ 10^{-4}$ ($7.2\ 10^{-4}$)	$1.6\ 10^{-3}$ ($0.7\ 10^{-3}$)	$2.6\ 10^{-5}$
Na^+	$2.5\ 10^{-5}$	$1.4\ 10^{-1}$ ($0.8\ 10^{-1}$)	$2.0\ 10^{-4}$ ($1.3\ 10^{-4}$)	$8.4\ 10^{-2}$ ($7.5\ 10^{-2}$)	$1.1\ 10^{-2}$ ($0.8\ 10^{-2}$)	$5.2\ 10^{-5}$
K^+	$5.0\ 10^{-6}$	$2.4\ 10^{-2}$ ($2.1\ 10^{-2}$)	$1.7\ 10^{-4}$ ($0.9\ 10^{-4}$)	$1.1\ 10^{-2}$ ($0.9\ 10^{-2}$)	$1.4\ 10^{-3}$ ($0.9\ 10^{-3}$)	$5.8\ 10^{-5}$
Si		$1.1\ 10^{-1}$ ($0.3\ 10^{-1}$)	$1.3\ 10^{-5}$ ($0.4\ 10^{-5}$)	$4.8\ 10^{-2}$ ($2.4\ 10^{-2}$)	$2.5\ 10^{-2}$ ($1.3\ 10^{-2}$)	$2.0\ 10^{-4}$
Al^{3+}		$1.5\ 10^{-4}$ ($0.6\ 10^{-4}$)	$3.6\ 10^{-7}$ ($1.9\ 10^{-7}$)	$1.2\ 10^{-7}$ ($1.1\ 10^{-7}$)	$2.0\ 10^{-4}$ ($2.0\ 10^{-6}$)	$0.2\ 10^{-6}$ - $1.1\ 10^{-6}$
Fe^{3+}		$1.7\ 10^{-4}$ ($0.9\ 10^{-4}$)	$3.6\ 10^{-7}$ ($3.5\ 10^{-7}$)	$2.0\ 10^{-7}$ ($0.9\ 10^{-7}$)	$4.4\ 10^{-3}$ ($2.4\ 10^{-3}$)	$4.5\ 10^{-5}$

[a] Honório et al. (2010)
[b] Barbiero et al. (2008, 2016)
[c] Rezende Filho et al. (2012), Fe value from Oliveira et al. (2019) and range of Al values from Förstner (1983)

3.2.3. Horizons minerals and organic matter

The field work of this study confirmed the data related to the geometry of the horizons given in previous studies (Barbiero et al., 2008; Furian et al., 2013), which allows us to propose a conceptual diagram of a typical soil sequence of an alkaline lake slope (Fig. 3). Minerals data related to clays are issued from Barbiero et al. (2008, 2016), Furquim et al. (2008, 2010a, 2010b). Upslope secondary aluminosilicates were mainly a ferribeidellite-type smectite, which is dioctaedral with mainly Al in the octahedral sheet, Fe-kaolinite and Fe-illite. In downslope horizons, the secondary smectite was of the stevensite type, which is trioctaedral with mainly Mg in the octahedral sheet. The given data allowed the calculation of the average chemical formula of these minerals, given in Table 2. Amorphous silica was observed all along the slopes, in the depth in upslope soils, where it accumulates to form a silcrete horizon just above the top of the dry season water table, and within the whole profile in the downslope soils, sometimes forming silcrete horizons outcropping the soil surface. In these studies, however, some data related to primary minerals were missing and certain secondary minerals predicted by PHREEQC were not mentioned. Consequently, we carried out complementary sampling.

3.3. Laboratory work

The soil pH was measured with a 1:2.5 w:w soil:water ratio. The XRD was conducted on powder samples. The fine fraction, <2 µm, was separated by sedimentation after destruction of the organic matter with NaOCl at pH 9.5 (Anderson; 1963). Oriented specimens were analysed by five different treatments: ethylene glycol solvation, Mg-saturation, K-saturation and heating of the K-saturated clay at 110 and 550°C (Wilson, 1987), using a CuKα radiation diffractometer with a graphite crystal monochromator. Analyses were run with a step size of 0.02 ° 2θ and a count time of 10 s per step. Soil particle size distribution was determined via the Robinson pipette method (Pansu and Gautheyrou, 2006).

3.4. The geochemical model

We used PHREEQC with the LLNL database (Johnson et al., 2000), which is the most complete database regarding soils minerals. The database was used in equilibrium mode because using kinetics mode would have required too many estimates of unknown parameters, such as specific surfaces and kinetic data for all minerals, to obtain reliable results. The minerals that were considered for modelling are given in Table 2. From the PHREEQC run results, we checked that no other possible minerals were left out in the script. We did not considered some sodic silicates such as kenyaite, magadiite and kanemite although they were indicated as possible in Barbiero et al. (2008) because they have never been observed in XRD results and are not included in the LLNL database.

Table 2
Composition of the minerals used in modelling.

Quartz SiO_2	Nahcolite $NaHCO_3$
K-feldspar $KAlSi_3O_8$	Gypsum $CaSO_4\ nH_2O$
Albite $NaAlSi_3O_8$	Alum-K $KAl(SO_4)_2\ 12\ H_2O$
Anorthite $CaAlSi_2O_8$	Epsomite $MgSO_4{\cdot}7\ H_2O$
Muscovite $KAl_2(AlSi_3O_{10})(OH)_2$	Gaylussite $Na_2Ca(CO_3)_2{\cdot}5\ H_2O$
Illite $[(Si_{3.5}Al_{0.5})O_{10}\ (Al_{1.8}\ Mg_{0.25})(OH)_2\ ]\ (K_{0.6})$	Glaserite $NaK_3(SO_4)_2$
Goethite FeO(OH)	Glauberite $Na_2Ca(SO_4)_2$
Amorphous silica $SiO_2\ nH_2O$	Halite NaCl
Ferribeidellite type smectite $[(Si_{3.18}Al_{0.82})O_{10}\ (Al_{1.69}\ Fe_{0.46}\ Mg_{0.04})(OH)_2\ ]\ (K_{0.05}\ Ca_{0.05}\ Mg_{0.07})$	Jarosite $KFe_3(SO_4)_2(OH)_6$
Stevensite type smectite $[(Si_4)O_{10}\ (Al_{0.12}\ Fe_{0.19}\ Mg_{2.3})(OH)_2\ ]\ (K_{0.05}\ Ca_{0.21})$	Mirabilite $Na_2SO_4{\cdot}10\ H_2O$
Fe-kaolinite $Si_2O_5(Al_{1.9}Fe_{0.1})(OH)_4$	Natron $Na_2CO_3{\cdot}10\ H_2O$
Fe-illite $[(Si_{3.61}\ Al_{0.39})O_{10}\ (Al_{0.62}\ Fe_{1.45})(OH)_2\ ]\ (K_{0.18})$	Pirssonite $Na_2Ca(CO_3)_2{\cdot}2\ H_2O$
Calcite $CaCO_3$	Sylvite KCl
Dolomite $CaMg(CO_3)_2$	Thenardite Na_2SO_4
	Trona $K_2NaH(CO_3)_2{\cdot}2\ H_2O$

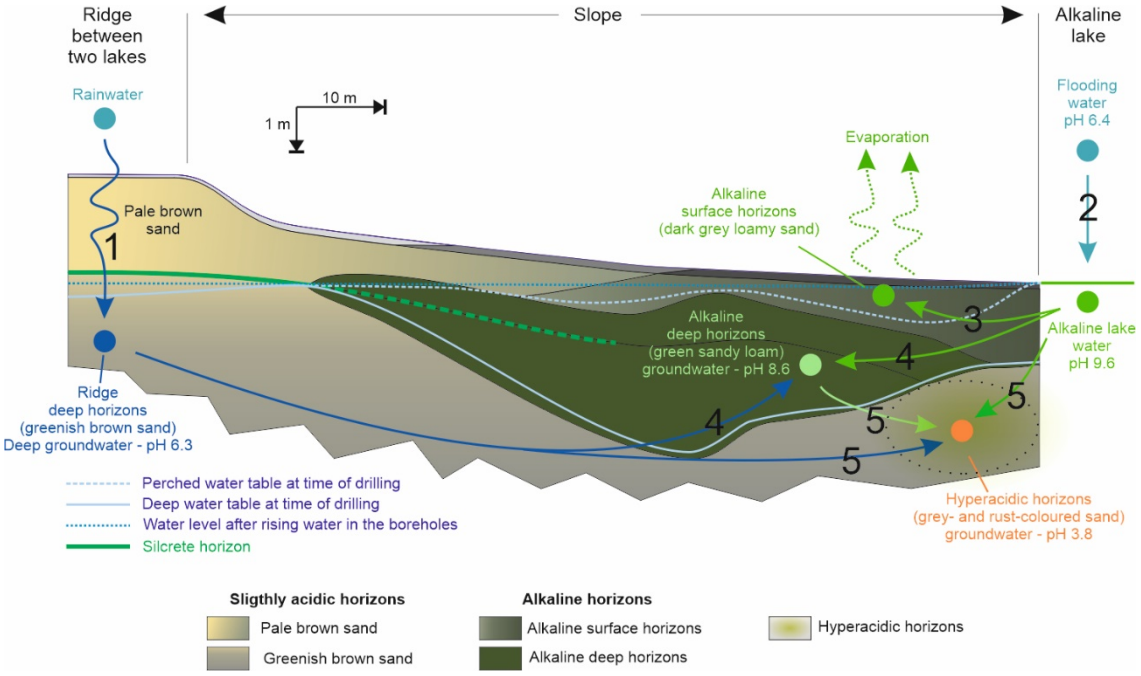

Fig. 3. Sketch of a typical soil sequence of an alkaline lake slope. Water-table levels are examples of dry season levels. Numbers in black on water fluxes refer to model number (Table 2).

Most stability constants (Ks) values were taken from the LLNL database. We used the illite value for Fe-illite and calculated the Ks values for Fe-kaolinite, ferribeidellite and stevensite after Tardy and Fritz (1981) and Tardy et al. (1987), using the LLNL values for kaolinite and goethite. The calculated Log(Ks) values were 6.54, 3.52 and 16.55 for Fe-kaolinite, ferribeidellite and stevensite, respectively. The values for Fe-kaolinite and ferribeidellite are close to the LLNL values for kaolinite and beidellite (6.81 and 4.63, respectively). The value for stevensite is lower than that (25.45) found by Chahi et al. (1997). We tested the sensibility of the model to such variations in the values of Ks. The results showed no or small differences, which do not modify the interpretations.

The models were defined taking into account our results related to the water tables and described below. In the ridge, rainwater percolates in depth during the rainy season and interacts with primary minerals to form the greenish brown sand horizons that constitute the aquifer of the deep groundwater (Fig. 3). During the dry season, the capillary rise of the deep groundwater is likely to form a silcrete horizon. On the slope, the green sandy loam with a low hydraulic conductivity isolates the deep groundwater from the water perched above. This perched groundwater can flow downslope in the rainy season, fed by rainwater and likely deep groundwater overflow. During the dry season, the perched water table is fed by the alkaline lake water that rises by capillarity. Beneath the green sandy loam, the hyperacidic horizon observed locally is likely to be formed by interaction between groundwaters from alkaline deep horizons, alkaline lakes and greenish brown sand.

These considerations have led us to define the five models described in Fig. 4, corresponding to the soil processes shown in Fig. 3. Model 1 corresponds to the pedogenesis on the ridge that is not impacted by annual flooding or by alkaline water capillary rising. Model 2 corresponds to the formation of the alkaline lake water from the flooding water and Model 3 to the genesis of the downslope surface horizons where occurs the evaporation of the alkaline lake water transferred by capillarity. Model 4 corresponds to the genesis of the green sandy loam horizon and Model 5 to the genesis of the grey- rust-coloured hyperacidic horizons.

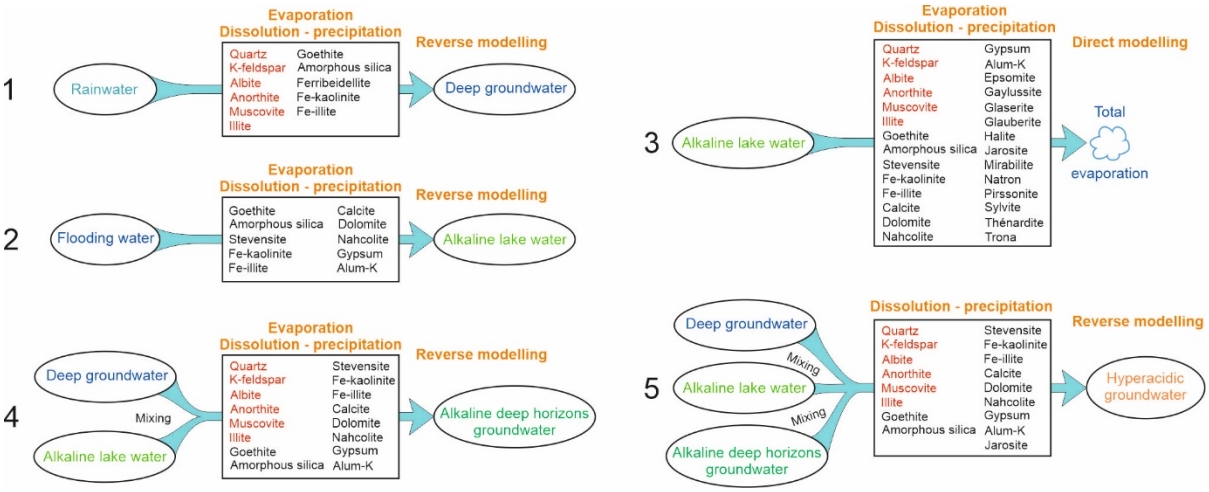

Fig. 4. Schedule of the 5 models. Mineral in red can only dissolve when minerals in black can dissolve and precipitate. In orange, processes taken into account and modelling type.

4. Results and discussion

4.1. Soil system and water table dynamics

The studied toposequence main features are given on Fig. 5. Vegetation was a semideciduous forest on the highest part of the toposequence which corresponds to the ridge between two lakes. The upper part of the slope was covered by an herbaceous vegetation becoming lower downslope; the lower part of the slopes, which corresponds to the most alkaline soils and which is periodically submerged, remained without vegetation. The geometry of horizons was close to that described in previous studies. Soil pH was neutral to slightly acidic in upslope soils, alkaline to very alkaline (up to more than 10) in the dark grey and greenish slope horizons. An hyperacidic horizon (pH 3.2) was observed downslope in depth, under the alkaline horizons (E horizon on Fig. 5). XRD data showed that quartz, K-feldspar (microcline, sanidine or orthoclase), muscovite, anorthite, albite and illite were present in all samples. Smectite-type clays were mainly dioctahedral (beidellite, montmorillonite type) in the upper slope soils (A and B horizons on Fig. 5) and trioctahedral (stevensite, saponite-type) in the downslope soils (C, D, F, G, H horizons). Calcite and K-alum were also observed in these latter horizons, whereas nahcolite was only observed in the D and F horizons. The soil features therefore correspond to the observations described in the literature and synthesized above in section 3.2 and to the conceptual diagram given in Fig. 3. Two separate water tables were observed during field work (Fig. 5): a deep, slightly acidic (pH<7) water table corresponding to the ridge deep groundwater (DG) in Table 1 and, at the lower part of the slope, the alkaline (pH>8.5) deep-horizons groundwater (ADHG) both within and perched above the green sandy loam horizon. During drilling, when the casing tube had entered the green sandy loam, groundwater did not enter the casing tube, which attests to the low hydraulic conductivity of the green sandy loam. Close to the lower limit of the green sandy loam, the deep groundwater slowly entered the casing tube, and when reaching the greenish brown sand, it was more rapid, rising to a level above that of the alkaline perched water table. These observations, already mentioned by Curti Martins (2012) for southeastern Nhecolândia, confirmed the disconnection between two types of groundwater. The interpretations given by Freitas et al. (2019), who do not consider a disconnection between groundwater tables and assume a permanent recharge of DG by ADHG, therefore do not apply to the soil system studied here. The hydraulic head of the deep groundwater was nearly constant at a given elevation all along the slope, which indicates that the deep groundwater of the boreholes belonged to the same aquifer, maybe regional but at least general at the landscape unit scale. These observations also show that the evapotranspiration of the ridge forest is not a process

that directly participate in the alkalinization of the ADHG, as has been observed by McCarthy and Ellery (1994) in the Okavango Delta which is a wetland of semi-arid area. In the Okavango delta, annual rainfall is 500 mm and potential evapotranspiration greatly exceeds rainfall each month of the year (Bauer et al., 2004). In the Nhecolândia, annual rainfall is 1100 mm and rainfall exceeds potential evapotranspiration from November to March for a total of about 210 mm (Hamilton et al., 1998), which is largely sufficient to leach out soluble species that may accumulate in forest soils during periods of water deficit.

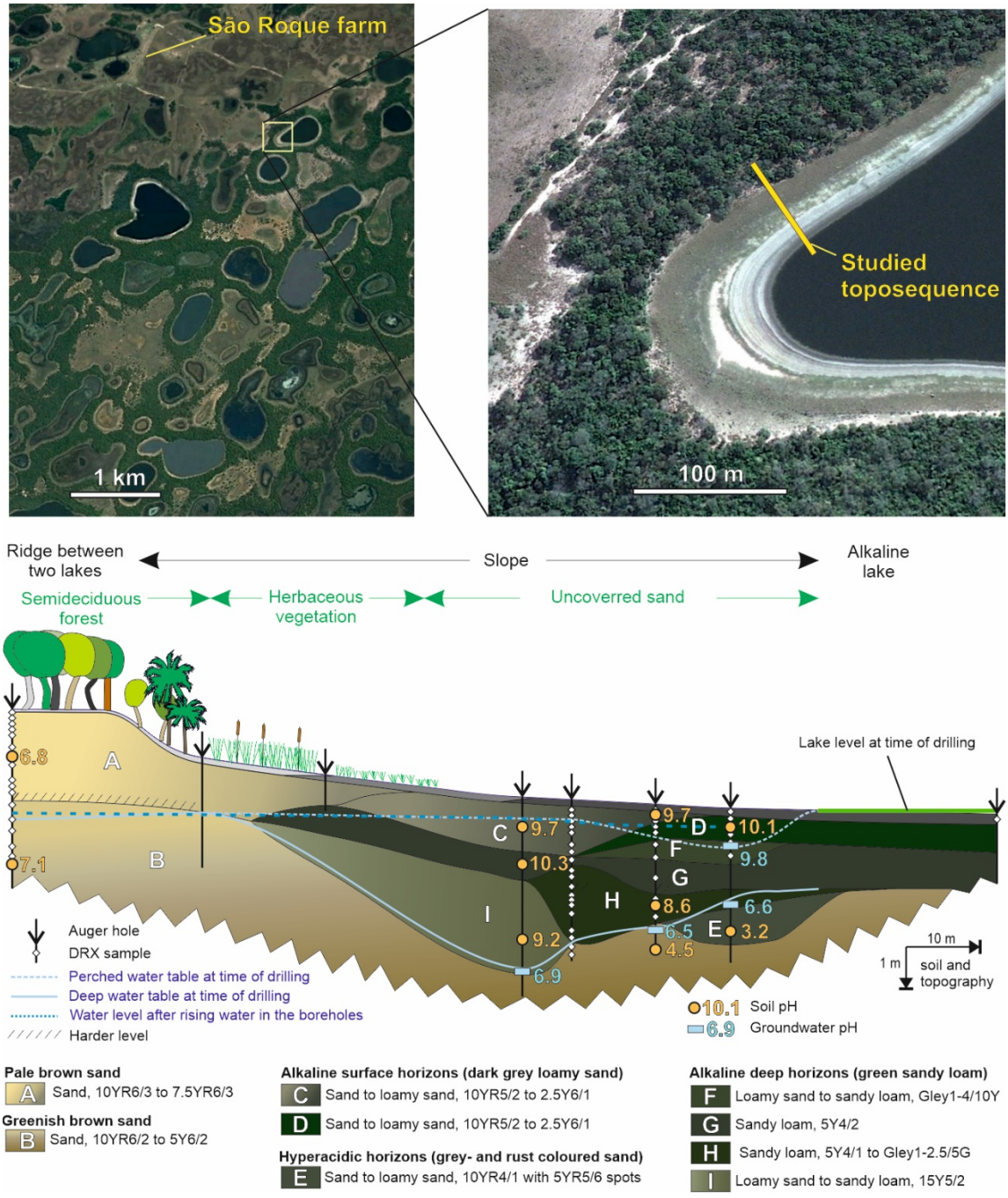

Fig. 5. Sketch of the studied soil sequence: situation in the landscape, topography, vegetation, main horizons geometry, colour and texture, water table depth, groundwater and soil pH.

4.2. Ridge pedogenesis – Model 1

The objectives of Model 1 were (1) to check, by reverse modelling, that the composition of the deep groundwater and the soil can be obtained by the dissolution of primary minerals and the precipitation of secondary minerals, (2) to provide rates of soil formation. The initial solution was the rainwater and the final solution was the deep groundwater. PHREEQC gave four results that solved the conditions imposed to the model (referred from a to d in Fig. 6), which all required the evaporation of 0.56 L of water per L of rainwater (evaporation factor, Ef). Evapotranspiration values are not available for the Pantanal, but this value is intermediate between the values available for cerrado (~ 50%) (Lima et al., 2001) and caatinga (~ 65%) (Felix and Paz, 2016) and therefore appears consistent with the ridge forest biome.

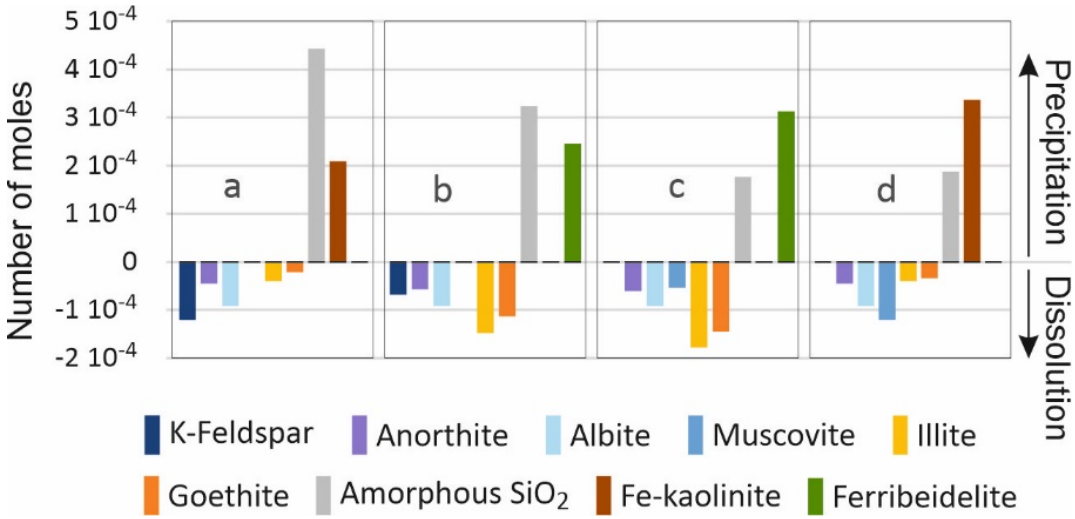

Fig. 6. Results of Model 1. Values corresponding to the formation of 1 L of deep groundwater. Numerical values are given in supplementary material.

All model results corresponded to the dissolution of muscovite or K-feldspar as a source of K and to the precipitation of Fe-kaolinite or ferribeidellite. Regarding primary minerals, dissolution rates at pH 5 and 25°C expressed in mol m^{-2} s^{-1} were 3.2 10^{-13} and 5.0 10^{-13} for muscovite and K-feldspar, respectively (Brantley, 2003; Köhler et al., 2003). These values are too close to each other to allow choosing between options, because the dissolution of muscovite, such as K-feldspar, likely occurs jointly. Regarding secondary minerals, both Fe-kaolinite and ferribeidellite were observed in the ridge deep horizons. In each of the model results, precipitation of amorphous silica occurred, which is consistent with the frequent occurrence of a silcrete-type horizon between the upper pale brown sand and the deep greenish brown sand.

The formation rate of ridge soils can be calculated from the model results, using the following hypotheses: (1) the parent material is mainly composed of quartz sand, with the few endogenous primary minerals that we considered in the modelling (quartz, K-feldspar, albite, anorthite, muscovite, illite) (Costa et al., 2015); (2) three types of horizons are formed: the pale brown sand, which is an eluvial horizon similar to the parent material but where primary minerals have been partially dissolved; the silcrete horizon, the site of precipitation of amorphous silica; the greenish brown horizon, where clay minerals – Fe-kaolinite and ferribeidellite – have precipitated. We know that the < 2µm fraction (fine fraction) in the greenish brown horizon consists of pedogenetic Fe-kaolinite and ferribeidellite, so we will consider any combination of two of the four solutions of Model 1, that would allow precipitation of both Fe-kaolinite and ferribeidellite.

In one m^3 of greenish brown horizon, the number of moles of Fe-kaolinite (Nv_K) and of ferribeidellite (Nv_B) are given by:

$$Nv_K = \frac{10\rho_a\, Ff\, R_{KB}}{M_K} \quad ; \quad Nv_B = \frac{10\rho_a\, Ff\, (1 - R_{KB})}{M_B} \tag{1}$$

where ρ_a is the bulk density in kg m^{-3}, Ff the fine fraction in weight %, R_{KB} the weight ratio Fe-kaolinite/ferribeidellite in the considered horizon and M_K, M_B are the molar mass in g of Fe-kaolinite and ferribeidellite, respectively. The number of moles of Fe-kaolinite (Ny_K) and of ferribeidellite (Ny_B) precipitated annually per m^2 predicted by the model are given by:

$$Ny_K = r_{modKB}\, Np_K\, R\, (1 - Ef) \quad ; \quad Ny_B = (1 - r_{modKB})\, Np_B\, R\, (1 - Ef) \tag{2}$$

where R is the annual rainfall, r_{modKB} is the ratio between the volumes of rainwater assigned to Fe-kaolinite and ferribeidellite precipitation, respectively and Np_K and Np_B are the number of moles of Fe-kaolinite and ferribeidellite precipitated respectively to generate 1L of deep groundwater (model result a or d for Fe-kaolinite precipitation, model result b or c for ferribeidellite precipitation on Fig. 6). The molar ratio Fe-kaolinite/ferribeidellite must be identical for the greenish brown sand and for the model result:

$$\frac{Nv_K}{Nv_B} = \frac{Ny_K}{Ny_b} \tag{3}$$

Replacing Nv_K, Nv_B, Ny_K, Ny_B by their expressions and simplifying, it comes:

$$r_{modKB} = \left(\frac{Np_K\, M_K\, (1 - R_{KB})}{Np_B\, M_B\, R_{KB}} + 1\right)^{-1} \tag{4}$$

Finally, the rate of formation Vg of the greenish brown sand, expressed in m y^{-1}, is given by:

$$V_g = \frac{Ny_K}{Nv_K} \tag{5}$$

To calculate the rate of soil formation r_{sf} (kg ha^{-1} y^{-1}) as considered, for example, by Wakatsuki and Rasyidin (1992), we have to consider also the number of moles of amorphous silica (Ny_S) precipitated annually per m^2:

$$Ny_S = (r_{modKB}\, Np_{Sk} + (1 - r_{modKB})\, Np_{Sb})\, R\, (1 - Ef) \tag{6}$$

where Np_{Sk} and Np_{Sb} are the number of moles of amorphous silica precipitated to generate 1L of deep groundwater and corresponding to model results precipitating Fe-kaolinite and ferribeidellite, respectively. The rate of soil formation is therefore given by:

$$r_{sf} = 10\,(Ny_k\,M_K + Ny_B\,M_B + Ny_S\,M_S) \quad (7)$$

where M_S is the molar mass in g of amorphous silica. Four pairs of the results given in Fig. 6 can be used to calculate the V_g and r_{sf} values: (a, c), (a, d), (b, c) and (b, d). The r_{sf} values obtained when using these four pairs ranged from 396 to 638 kg ha^{-1} y^{-1}. These values are of the same order of magnitude as the soil formation rates obtained with other approaches. For example, the average rate of soil formation at the global scale was estimated at around 695 kg ha^{-1} y^{-1} (Wakatsuki and Rasyidin, 1992), and the soil formation rate on landscape ridges in a semi-arid Australian area was estimated to be approximately 530 kg ha^{-1} y^{-1} (Yoo et al., 2007).

The rate of formation V_g of the greenish brown sand was calculated using the particle size distribution and the bulk density values shown in Table 3. The obtained range was 4.8 10^{-4} to 1.1 10^{-3} m y^{-1}, which corresponds 949 to 2,090 years to form 1 m of horizon. This high formation rate is due to the low clay content of the horizon, with the time of formation being proportional to the clay content. This estimate is consistent with palynological data of Becker et al. (2018), which shows that an alkaline lake equivalent to the one studied here has been operating for about 3300 y.

Table 3
Particle size distribution and bulk density (ρ_a) of the studied horizons. *Ff* : fine fraction, < 2 µm. Avg: average. Std: standard deviation.

	Sand		Silt		*Ff*		ρ_a
	avg	std	avg	std	avg	std	
	weight %						kg ha^{-1} y^{-1}
Pale brown sand (n = 15)	95.3	1.0	4.1	0.6	0.7	0.3	1300
Greenish brown sand (n = 6)	92.9	4	3.4	2.2	3.7	1.7	1500
Green sandy loam (n = 11)	83.4	3.5	4.5	1.8	12.1	1.4	1500
Dark grey sandy loam (n = 18)	95.0	3.2	3.5	2.9	1.4	0.9	1380
Grey- rust coloured sand (n=1)	95.5	/	4.0	/	0.5	/	1400

4.3. From flooding water to alkaline lake water – Model 2

Here, we used PHREEQC to identify, by reverse modelling, the required conditions to obtain the alkaline lake water from the flooding water. When setting the dissolved Al value of the flooding water to the upper limit of the interval shown in Table 1 (1.1 10^{-6} mol L^{-1}), the model proposed six results with small differences in the amount of precipitated minerals. Considering the result with the lower sum of residuals, Ef was equal to 0.9990, and the precipitated quantities in moles corresponding to the formation of 1 L of alkaline lake water were 2.41 10^{-3}, 4.24 10^{-3}, 9.42 10^{-4} and 7.78 10^{-2} for stevensite, calcite, dolomite and amorphous silica, respectively. All these minerals were

observed in the downslope soils and in the alkaline lake sediment. The Si was controlled by the precipitation of stevensite and amorphous silica. A change in the ratio between these minerals changed the amount of Ca and Mg precipitated in the stevensite, which was offset by a change in the ratio between calcite and dolomite precipitation. All results required a high evaporation, with the Ef value corresponding to the evaporation of more than 985 L of flooding water per L of alkaline lake water. When setting the dissolved Al value of the flooding water to lower values, down to the lower limit of the interval shown in Table 1 (0.2 10^{-6} mol L^{-1}), the model progressively reduced the amount of Al-bearing mineral without changing the concentration factor by more than 0.5%.

Such a concentration factor cannot be achieved by evaporation in a lake between flooding and the dry season. We used an average alkaline lake to calculate the order of magnitude of evaporation in 1 year. For this, we considered a circular lake with a radius of 140 (Costa et al., 2015) to 100 m from the wet to the dry season and a flat bottom below the surface of the lake submerged during the dry season. This morphology is simplified compared to the observations of Barbiero et al. (2016), who specified that the edges of alkaline lakes are generally deeper than the centre, but this has no influence on the balance established below. On average, 1.5 m of water evaporated from the wet to the dry season (Alho, 2008), with 0.3 m of water remaining in the dry season. Based on these data, the lake slopes are 3.75 % and the lake water volumes are 77,178 and 8,691 m^3 in the wet and the dry season, respectively, corresponding to the evaporation of 7.9 L of flooding water per L of alkaline lake water. This value is 125 times smaller than the value (985 L) necessary to obtain the chemistry of the lake water, according to the modelling. This leads us to infer that such a process must be repeated for 125 years without losses to explain the concentrations currently observed.

This result reinforces the hypothesis first provided in Barbiero et al. (2002). During the dry season, labile elements are transferred by capillary action and precipitate in the downslope surface horizons. During flooding, these precipitates are dissolved, with the labile elements being leached laterally toward the lake by the sub-superficial groundwater. The calculated duration of 125 years necessary for the accumulation of labile species is obviously underestimated, because it does not consider losses during the rainy season, for the estimation of which additional studies would be necessary.

4.4. Mineral precipitations in the downslope surface horizons – Model 3

The objective was to identify the minerals likely to precipitate when the alkaline lake water concentrates by evaporation in these horizons. The PREEQC model was used in direct modelling. This model simulates the progressive evaporation of an average alkaline lake water that rises by capillarity in the downslope surface horizons during the dry season; results are shown in Fig. 7. Up to the evaporation of 92% of the initial water, amorphous silica, calcite and dolomite are the only precipitated minerals. From 95% onward, calcite and, partially, amorphous silica redissolve due to ionic strength and the pH increase; Ca with Na precipitate in gaylussite which is in turn replaced by pirssonite from 96% of evaporation. In the last stages sylvite, nahcolite, halite and glaserite precipitate. This set of minerals is therefore able to buffer the alkaline lake chemistry. Among these minerals, calcite, dolomite and nahcolite were the only ones identified by XRD in the downslope surface horizons. Regarding the other minerals, the XRD detection limit (1–5% or more by volume, depending on the mineral and its crystallinity) was likely too high to allow identification of small amounts in raw samples; in the clay fraction, these minerals were probably dissolved during aqueous phase extraction.

Such minerals, however, can store labile species during the dry season, avoiding an excessive alkalinisation of the lake and allowing the maintenance of an important microalgal activity and their high solubilities allow maintaining a high alkalinity of the lake when it is filled by the perched water tables of the slopes. This result strengthens the conclusion issued from Model 2.

A consequence of such a dynamic system is that the alkaline character of the lakes can disappear very quickly if new drainage conditions allow an export of the labile elements out of the system. This is likely what occurred in the soil systems studied by Oliveira Junior et al. (2020) in Northern

Pantanal, where alkaline soils leached and acidified as a result of a change in flooding dynamics. This was also hypothesized in Furquim et al. (2017).

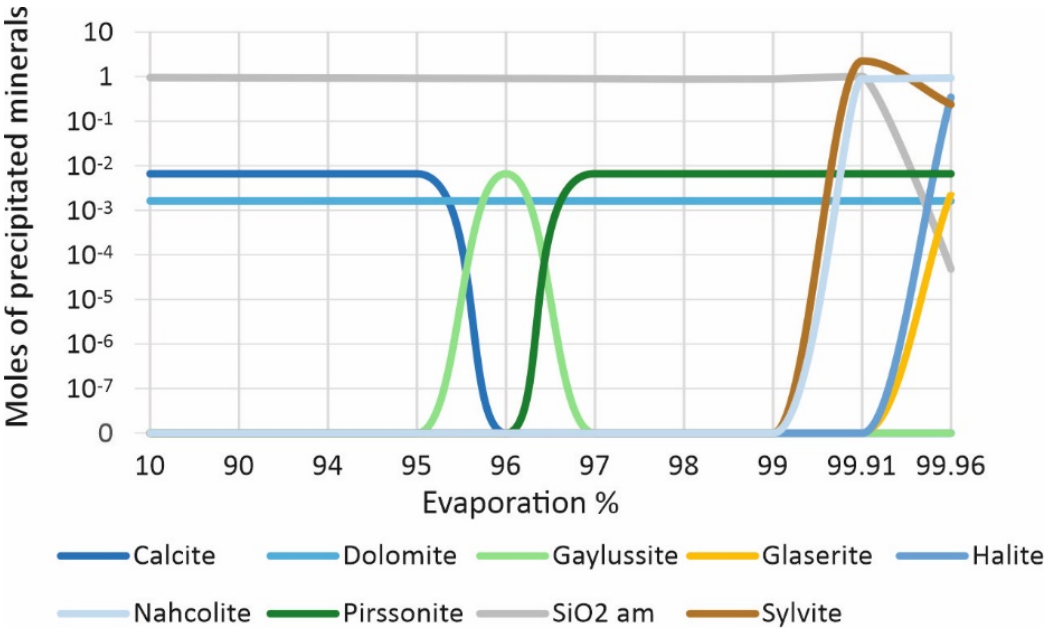

Fig. 7. Results of Model 3. Values corresponding to the evaporation of 10 L of an average alkaline lake water. Numerical values are given in supplementary material.

4.5. Genesis of the green sandy loam horizons – Model 4

Here, PHREEQC was used by reverse modelling to evaluate if a mixing between alkaline lake water and deep groundwater can allow the precipitation of the green sandy loam horizon minerals. We considered the interaction of a mixture of 0.56 L of average alkaline lake water with 0.44 L of deep groundwater with the minerals given in Table 2 to obtain the alkaline deep horizons groundwater. The mixing ratio was obtained from mass-balance of the chloride, considered as an inert, non-reactive tracer. Even using the lowest uncertainty values for species involved in mineral-solution balances, the model yielded more than 50 possible results, without the need for water evaporation. Most similar, these results can be grouped into six types. For each type, the result with the lowest sum of residuals is given in Fig. 8.

In all solutions, quartz or amorphous SiO_2, goethite and ferribeidellite were dissolved; stevensite and Fe-illite were precipitated. In some solutions, Fe-kaolinite and calcite were also dissolved and nahcolite and dolomite were precipitated. Sulphates were controlled by precipitation of alum-K because gypsum is highly unlikely in such an alkaline medium. These results are consistent with mineralogical observations, demonstrating that the green sandy loam horizons currently forms by interaction between the minerals observed in the greenish brown sand, the deep groundwater and the alkaline lake water. They agree with all detailed studies carried out on the morphology of the soil system surrounding the alkaline lakes. All authors mentioned a strengthening of the thickness of this greenish brown horizon close to the contact zone between the alkaline waters and the deep groundwaters (Sakamoto, 1997; Barbiero et al., 2008; Furquim et al., 2010b; Curti Martins, 2012). It should be noted that if the supply of Si and K for the reaction takes place directly in dissolved form, the supply of Fe and Al takes place via complexation with organic forms (Barbiero et al., 2016), which explains the coexistence of Fe-illite and Mg smectites a few meters apart within the same soil system.

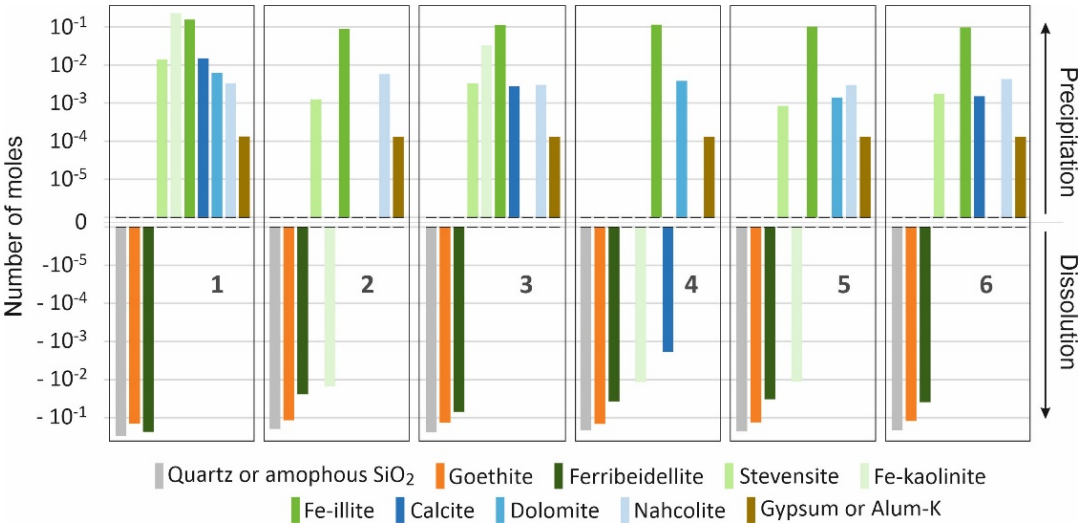

Fig. 8. Results of Model 4: number of moles of minerals dissolved (negative values) or precipitated (positive values) to satisfy the model conditions. For gypsum and alum-K, number of moles is the number of SO_4 groups. Numerical values are given in supplementary material.

4.6. Genesis of the grey- rust-coloured hyperacidic horizons – Model 5

These horizons were observed in the depth at the lower part of the toposequences (Fig. 3), in places where alkaline, reducing water (ADHG or ALW, see Table 1) can mix with oxidizing deep groundwater with a lower pH (DG). The objective was to understand if, and how, such a horizon can be formed by mixing between these types of water without gas exchange with the atmosphere. In a first attempt, PHREEQC was used in reverse modelling, using mixtures of groundwater, with a ratio given by chloride mass-balance, as the initial solution interacting with the green sandy loam minerals to form the hyperacidic groundwater. This attempt, however, did not yield a solution, most likely because of too much uncertainty on the composition of the hyperacid groundwater, which was only defined from five samples.

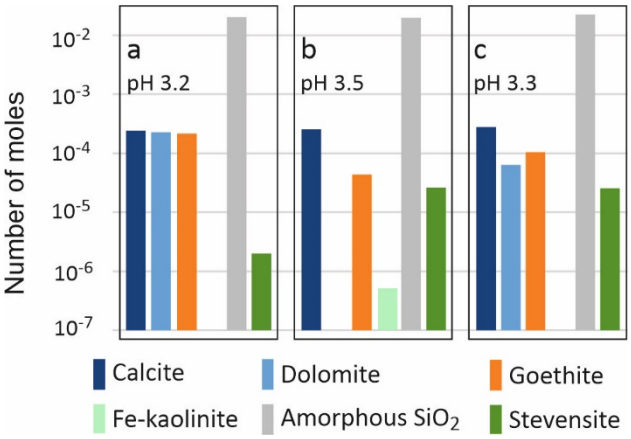

Fig. 9. Results of Model 5. Obtained pH and number of moles precipitated for 1 L of mixture. Numerical values are given in supplementary material.

In a second step, PHREEQC was used in direct mode to model what occurs when the three types of water are mixed without gas exchange with the atmosphere. We used the three mixing scenarios which consider the chloride mass balance: a: 50% DG + 50% ADHG; b: 72% DG + 28% ADHG; c: 64%

DG, 18% ADHG, 18% ALW. The results were close to each other (Fig. 9). In scenarios a and c the mixing of the water causes the precipitation of calcite, amorphous SiO_2, dolomite, goethite and stevensite; in scenario b dolomite was not precipitated but Fe-kaolinite was. In all cases the pH was drastically reduced, due to the consumption of OH^- by the precipitation of clay minerals and, especially, of goethite (ferrolysis, Brinkman, 1970), as shown by the following reactions.

$$0.05\ K^+ + 0.12\ Al^{3+} + 2.3\ Mg^{2+} + 0.19\ Fe^{3+} + 0.21\ Ca^{2+} + 4\ Si(OH)_4 \Leftrightarrow \text{stevensite } [(Si_4)O_{10}\ (Al_{0.12}\ Fe_{0.19}\ Mg_{2.3})(OH)_2\ ]\ (K_{0.05}\ Ca_{0.21}) + 4\ H_2O + 6\ H^+$$

$$1.9\ Al^{3+} + 0.1\ Fe^{3+} + 2\ Si(OH)_4 + H_2O \Leftrightarrow \text{Fe-kaolinite } Si_2O_5(Al_{1.9}Fe_{0.1})(OH)_4 + 6\ H^+$$

$$Fe^{3+} + 2\ H_2O \Leftrightarrow \text{goethite } FeO(OH) + 3\ H^+$$

This result is consistent with the field and mineralogical observations, which have shown goethite precipitation related to the rust colour in the hyperacidic horizon. We did not consider, however, a possible role of chlorides and organochlorines in the hyperacidification process. Taking into account this type of species with their complex interactions linked to the redox conditions, in particular with Fe (Vodyanitskii and Makarov, 2017), must be the subject of complementary works.

5. Conclusions

We confirmed the disconnection between two types of groundwater in the surroundings of alkaline lakes, almost disconnected from each other: a deep water table slightly acidic, widespread at the landscape unit scale and, at the lower part of the slope, an alkaline water table perched above the impervious horizons.

The simulations carried out showed that the presently observed soil paragenesis can be obtained by the current biogeochemistry. It is not necessary to assume characters inherited from dryer paleoclimates to explain the soils currently observed. They showed the consistency between the mineralogy of the horizons and the present-days chemistry of the water tables, verifying the geochemical hypothesis that downslope soils act as buffers to store labile species during the dry season, which avoids an excessive alkalinisation of the lakes and facilitates the maintenance of an important microalgal activity. This also explains the variability of the lakes, with their alkalinity being the result of local hydrodynamics: alkaline lakes can only develop where pedogenic horizons constitute thresholds which prevent the alkaline waters from leaching out of the system. Given the highly dynamic nature of the system, the alkaline character of the lakes can disappear quickly if new drainage conditions allow an export of the labile elements out of the system.

The simulations also made it possible to quantify some of the processes that act in the soil system:

- The ridge soil formation rate ranges from 396 to 638 kg ha^{-1} y^{-1}, depending on the hypotheses.
- To reach the alkaline nature of the lakes, a minimum of 125 years is required.

Finally, simulations have shown that the large acidity contrast between alkaline deep horizons and hyperacid horizons can be simply explained by contact and mixing of the slightly acidic deep groundwater with the alkaline waters of the alkaline deep horizons or of the alkaline lakes; the pH decrease is mainly related to goethite precipitation. Further works, however, will be necessary to determine the potential role of chlorides, organic matter and organochlorines.

Acknowledgements

The authors thank D.L. Parkhurst for his valuable insights into the intricacies of the PHREEQC code.

Funding

This work was supported by the São Paulo Research Foundation (FAPESP) [grant number #2016/14227-5, doctoral scholarship #2019/21157-1]; the National Council for Scientific and Technological Development (CNPq) [research scholarship to CRM #307024/2018-0]; and National Institute of Sciences of the Universe (INSU-CNRS) [Ec2co Pantanal project].

References

Alho, C.J.R., 2008. Biodiversity of the Pantanal: response to seasonal flooding regime and to environmental degradation. Braz. J. Biol. 68, 957–966. https://doi.org/10.1590/S1519-69842008000500005

Almeida, T.I.R., Karmann, I., Paranhos Filho, A.C., Sígolo, J.B., Bertolo, R.A., 2010. Os diferentes graus de isolamento da água subterrânea como origem de sua variabilidade: evidências isotópicas, hidroquímicas e da variação sazonal do nível da água no Pantanal da Nhecolândia. Geol. USP 10(3), 37-47. http://dx.doi.org/10.5327/Z1519-874X2010000300003

Anderson, J.U., 1963. An improved pretreatment for mineralogical analysis of samples containing organic matter. Clays Clay Miner. 10, 380–388. https://doi.org/10.1346/CCMN.1961.0100134

Andreote, A.P.D., Vaz, M.G.M.V., Genuário, D.B., Barbiero, L., Rezende-Filho, A.T., Fiore, M.F., 2014. Nonheterocytous cyanobacteria from Brazilian saline-alkaline lakes. J. Phycol. 50, 675-684. http://dx.doi.org/10.1111/jpy.12192

Assine, M.L., Merino, E.R., Pupim, F.N., Warren, L.V., Guerreiro, R.L., McGlue, M.M., 2015. Geology and Geomorphology of the Pantanal Basin, in: Bergier, I., Assine, M. (Eds), Dynamics of the Pantanal Wetland in South America. The Handbook of Environmental Chemistry 37. Springer, Cham, pp. 23-50. https://doi.org/10.1007/698_2015_349

Barbiero, L., de Queiroz Neto, J.P., Ciornei, G., Sakamoto, A.Y., Capellari, B., Fernandes, E., Valles, V., 2002. Geochemistry of water and ground water in the Nhecolândia, Pantanal of Mato Grosso, Brazil: variability and associated processes. Wetlands 22, 528-540. https://doi.org/10.1672/0277-5212(2002)022[0528:GOWAGW]2.0.CO;2

Barbiero, L., Filho, A.R., Furquim, S.A.C., Furian, S., Sakamoto, A.Y., Valles, V., Graham, R.C., Fort, M., Ferreira, R.P.D., Neto, J.P.Q., 2008. Soil morphological control on saline and freshwater lake hydrogeochemistry in the Pantanal of Nhecolândia, Brazil. Geoderma 148, 91-106. https://doi.org/10.1016/j.geoderma.2008.09.010

Barbiero, L., Kumar, M.S.M., Violette, A., Oliva, P., Braun, J.J., Kumar, C., Furian, S., Babic, M., Riotte, J., Valles, V., 2010. Ferrolysis induced soil transformation by natural drainage in Vertisols of sub-humid South India. Geoderma 156, 173-188. https://doi.org/10.1016/j.geoderma.2010.02.014

Barbiero, L., Berger, G., Rezende Filho, A.T., Meunier, J.F., Martins-Silva, E.R., Furian, S., 2016. Organic Control of Dioctahedral and Trioctahedral Clay Formation in an Alkaline Soil System in the Pantanal Wetland of Nhecolândia, Brazil. PLoS One 11, e0159972. https://doi.org/10.1371/journal.pone.0159972

Barbiero, L., Siqueira Neto, M., Braz, R.R., Carmo, J.B.d., Rezende Filho, A.T., Mazzi, E., Fernandes, F.A., Damatto, S.R., Camargo, P.B.d., 2018. Biogeochemical diversity, O2-supersaturation and hot moments of GHG emissions from shallow alkaline lakes in the Pantanal of Nhecolândia, Brazil. Sci. Tot. Env. 619-620, 1420-1430. https://doi.org/10.1016/j.scitotenv.2017.11.197

Bauer, P., Thabeng,G., Stauffer, F., Kinzelbach, W., 2004. Estimation of the evapotranspiration rate from diurnal groundwater level fluctuations in the Okavango Delta, Botswana. J. Hydrol. 288, 344-355. https://doi.org/10.1016/j.jhydrol.2003.10.011

Becker, B.F., da Silva-Caminha, S.A.F., Guerreiro, R.L., de Oliveira, E.J., D'Apolito, C., Assine, M.L., 2018. Late Holocene palynology of a saline lake in the Pantanal of Nhecolândia, Brazil. Palynology 42, 457–465. https://doi.org/10.1080/01916122.2017.1386843

Bergier, I., Krusche, A., Guérin, F., 2014. Alkaline lake dynamics in the Nhecolândialandscape, in: Bergier, I., Assine, M.L. (Eds.), Dynamics of the Pantanal Wetland in South America. The Handbook of Environmental Chemistry 37. Springer, Cham, pp. 145–161. https://doi.org/10.1007/698_2014_327

Brantley, S.L., 2003. 5.03 -Reaction Kinetics of Primary Rock-forming Minerals under Ambient conditions, in: Heinrich D.H., Karl K.T. (Eds.), Treatise on Geochemistry. Pergamon Press, Oxford, pp. 73-117. https://doi.org/10.1016/B0-08-043751-6/05075-1

Brinkman, R., 1970. Ferrolysis, a hydromorphic soil forming process. Geoderma 3, 199-206. https://doi.org/10.1016/0016-7061(70)90019-4

Chahi, A., Fritz, B., Duplay, J., Weber, F., Lucas, J., 1997. Textural transition and genetic relationship between precursor stevensite and sepiolite in lacustrine sediments (Jbel Rhassoul, Morocco). Clays Clay Min. 45, 378-389. https://doi.org/10.1346/CCMN.1997.0450308

Costa, M., Telmer, K.H., Evans, T.L., Almeida, T.I.R., Diakun, M.T., 2015. The lakes of the Pantanal: inventory, distribution, geochemistry, and surrounding landscape. Wetlands Ecol. Manage. 23, 19–39. https://doi.org/10.1007/s11273-014-9401-3

Curti Martins, E.R., 2012. Tipologias de lagoas salinas no Pantanal da Nhecolândia (MS). Thesis, Universidade de São Paulo, 188 p. http://doi.org/10.11606/T.8.2012.tde-14012013-172446

Felix, V.S., Paz, A.R., 2016. Hydrological processes representation in a semiarid catchment located in Paraiba state with distributed hydrological modelling. Braz. J. Wat. Res. 21, 556-569. https://doi.org/10.1590/2318-0331.011616009

Förstner, U., 1981. Metal Concentrations in River, Lake, and Ocean Waters, in: Förstner, U., Wittmann, G.T.W. (Eds.), Metal Pollution in the Aquatic Environment. Springer Verlag, Berlin, Heidelberg, pp. 71-109. https://doi.org/10.1007/978-3-642-69385-4_3

Feder, F., Trolard, F., Bourrié, G., Klingelhöfer, G., 2018. Quantitative estimation of fougerite green rust in soils and sediments by citrate—bicarbonate kinetic extractions. Soil Systems 2, 54-66.
https://doi.org/10.3390/soilsystems2040054

Freitas, J.G., Furquim, S.A.C., Aravena, R., Cardoso, E.L., 2019. Interaction between lakes' surface water and groundwater in the Pantanal wetland, Brazil. Env. Earth Sci. 78, 139. https://doi.org/10.1007/s12665-019-8140-4

Furian, S., Martins, E.R.C., Parizotto, T.M. Rezende, A.T., Victoria, R.L., Barbiero, L., 2013. Chemical diversity and spatial variability in myriad lakes in Nhecolandia in the Pantanal wetlands of Brazil. Limnol. Oceanogr. 58, 2249–61. https://doi.org/10.4319/lo.2013.58.6.2249

Furquim, S.A.C., Graham, R.C., Barbiero, L., Neto, J.P.D., Valles, V., 2008. Mineralogy and Genesis of Smectites in an Alkaline-Saline Environment of Pantanal Wetland, Brazil. Clays Clay Min. 56, 579–95. https://doi.org/10.1346/Ccmn.2008.0560511

Furquim, S.A.C., Graham, R.C., Barbiero, L., Neto, J.P.Q., Vidal-Torrado, P., 2010a. Soil mineral genesis and distribution in a saline lake landscape of the Pantanal Wetland, Brazil. Geoderma 154, 518–28. https://doi.org/10.1016/j.geoderma.2009.03.014

Furquim, S. A. C., Barbiero, L., Graham, R.C., Queiroz Neto, J.P., Ferreira, R.P.D., Furian, S., 2010b. Neoformation of micas in soils surrounding an alkaline–saline lake of Pantanal wetland, Brazil. Geoderma 158, 331–342. https://doi.org/10.1016/j.geoderma.2010.05.015

Furquim, S.A.C., Santos, M.A., Vidoca, T.T., Balbino, M.A., Cardoso, E.L., 2017. Salt-affected soils evolution and fluvial dynamics in the Pantanal wetland, Brazil. Geoderma 286, 139–152. http://dx.doi.org/10.1016/j.geoderma.2016.10.030

Guerreiro, R.L., Bergier, I., McGlue, M.M., Warren, L.V., Abreu, U.G.P.d., Abrahão, J., Assine, M.L., 2019. The soda lakes of Nhecolândia: A conservation opportunity for the Pantanal wetlands. Perspect. Ecol. Conserv. 17, 9-18. https://doi.org/10.1016/j.pecon.2018.11.002

Hamilton, S.K., Souza, O.C., Coutinho, M.E., 1998. Dynamics of floodplain inundation in the alluvial fan of the Taquari River (Pantanal, Brazil). SIL Proc. 1922-2010 26, 916-922. https://doi.org/10.1080/03680770.1995.11900852

Honório, B.A.D., Horbe, A.M.C., Seyler, P., 2010. Chemical composition of rainwater in western Amazonia — Brazil. Atmos. Res. 98, 407-425. https://doi.org/10.1016/j.atmosres.2010.08.001

Huang, L. M., Zhang, G.L., Yang, J.L., 2013. Weathering and soil formation rates based on geochemical mass balances in a small forested watershed under acid precipitation in subtropical China. Catena 105, 11-20. https://doi.org/10.1016/j.catena.2013.01.002

Johnson, J., Anderson, F., Parkhurst, D.L., 2000. Database thermo.com.V8.R6.230, Rev 1.11. Lawrence Livermore National Laboratory, Livermore, California.

Köhler, S.J., Dufaud, F., Oelkers, E.H., 2003. An experimental study of illite dissolution kinetics as a function of ph from 1.4 to 12.4 and temperature from 5 to 50°C. Geoch. Cosmoch. Acta 67, 3583-3594. https://doi.org/10.1016/S0016-7037(03)00163-7

Lecomte, K.L., Pasquini, A.I., Depetris, P.J., 2005. Mineral Weathering in a Semiarid Mountain River: Its assessment through PHREEQC inverse modeling. Aquatic Geochem. 11, 173-194. https://doi.org/10.1007/s10498-004-3523-9

Lima, J.E.F.W., Silva, C.L., Oliveira, C.A.S., 2001. Comparação da evapotranspiração real simulada e observada em uma bacia hidrográfica em condições naturais de cerrado. Rev. Bras. Eng. Agr. Amb. 5, 33-41. https://doi.org/10.1590/S1415-43662001000100007

Maglione, G., 1974. Géochimie et mécanismes de mise en place actuelle des évaporites dans le bassin tchadien. Bulletin de Liaison - ASEQUA 42-43, 33-44.

Marengo, J.A., Oliveira, G.S., Alves, L.M., 2015. Climate Change Scenarios in the Pantanal, in: Bergier, I., Assine, M. (Eds), Dynamics of the Pantanal Wetland in South America. The Handbook of Environmental Chemistry 37. Springer, Cham, pp. 227-238. https://doi.org/doi:10.1007/698_2015_357

Mathian, M., Aufort, J., Braun, J.J., Riotte, J., Selo, M., Balan, E., Fritsch, E., Bhattacharya, S., Allard,T., 2019. Unraveling weathering episodes in Tertiary regoliths by kaolinite dating (Western Ghats, India). Gondwana Res. 69, 89-105. https://doi.org/10.1016/j.gr.2018.12.003

McCarthy, T.S., Metcalfe, J., 1990. Chemical sedimentation in the semi-arid environment of the Okavango Delta, Botswana. Chem. Geol. 89, 157-178. https://doi.org/10.1016/0009-2541(90)90065-F

McCarthy, T.S., Ellery, W.N., 1994. The effect of vegetation on soil and ground water chemistry and hydrology of islands in the seasonal swamps of the Okavango fan, Botswana. J. Hydrol. 154, 169-193. https://doi.org/10.1016/0022-1694(94)90216-X

Oliveira, M.D., Calheiros, D.F., Hamilton, S.K., 2019. Mass balances of major solutes, nutrients and particulate matter as water moves through the floodplains of the Pantanal (Paraguay River, Brazil). Rev. Bras. Rec. Hydr. 24, e1. https://doi.org/10.1590/2318-0331.231820170169

Oliveira Junior, J.C., Andrade, G.R.P., Barbiero, L., Furquim, S.A.C., Vidal-Torrado, P., 2020. Flooding effect on mineralogical and geochemical changes in alkaline-sodic soil system of northern Pantanal wetlands, Brazil. Eur. J. Soil Sci. 71, 433– 447. https://doi.org/10.1111/ejss.12871

Pansu, M., Gautheyrou, J., 2006. Particle Size Analysis, in: Handbook of Soil Analysis. Springer, Berlin, Heidelberg, pp. 15-63. https://doi.org/10.1007/978-3-540-31211-6_2

Parkhurst, D.L., Appelo, C.A.J., 2013. Description of input and examples for PHREEQC version 3—a computer program for speciation, batch-reaction, one-dimensional transport, and inverse geochemical calculations. US Geological Survey Techniques and Methods, Book 6, chap A43, 497 p. http://pubs.usgs.gov/tm/06/a43

Pereira, O.J.R., Merino, E.R., Montes, C.R., Barbiero, L., Rezende-Filho, A.T., Lucas, Y., Melfi, A.J., 2020. Estimating Water pH Using Cloud-Based Landsat Images for a New Classification of the

Nhecolândia Lakes (Brazilian Pantanal). Remote Sens. 12, 1090. https://doi.org/10.3390/rs12071090

Rezende Filho, A.T., Furian, S., Victoria, L.R., Mascré, C., Vallès, V., Barbiero, L., 2012. Hydrochemical variability at the Upper Paraguay Basin and Pantanal wetland. Hydrol. Earth Syst. Sci. 16, 2723–2737. https://doi.org/10.5194/hess-16-2723-2012

Salis, S.M., Lehn, C.R., Mattos, P.P., Bergier, I., Crispim, S.M.A., 2014. Root behavior of savanna species in Brazil's Pantanal wetland. Glob. Ecol. Conserv. 2, 378-384. https://doi.org/10.1016/j.gecco.2014.10.009

Sakamoto, A.Y., 1997. Dinâmica hídrica em uma lagoa salina e seu entorno no Pantanal da Nhecolândia: contribuição ao estudo das relações entre o meio físico e a ocupação, Fazenda São Miguel do Firme. Thesis, Universidade de São Paulo, 165 p.

Schmidt, C., Zöller, L., Hambach, U.F., 2015. Dating of sediments and soils, in: Lucke, B., Bäumler, R., Schmidt, M. (Eds.), Soils and Sediments as Archives of Environmental Change. Geoarchaeology and Landscape Change in the Subtropics and Tropics, Erlanger Geographische Arbeiten 42, Erlangen, pp. 119-146.

Tardy, Y, Fritz, B. 1981. An ideal solid solution model for calculating solubility of clay minerals. Clay Miner. 16, 361- 373. https://doi.org/10.1180/claymin.1981.016.4.05

Tardy, Y, Duplay, J., Fritz, B., 1987. Stability fields of smectites and illites as a function of temperature and chemical composition. SKB Tech. Rep. 87-20. SKB Svensk Kärnbräns-lehantering AB, Stockholm, Sweden, 38 p.

Van Bennekom, A.J., Jager, J.E., 1978. Dissolved aluminium in the Zaire river plume. Neth. J. Sea Res. 12, 358-367.

Valles, V., N'Diaye, M., Bernadac, A., Tardy, Y. 1989. Geochemistry of waters in the Kouroumari region, Mali; Al, Si, and Mg in waters concentrated by evaporation: Development of a model. Arid Soil Res. Rehab. 3, 21-39. https://doi.org/10.1080/15324988909381186

Vodyanitskii, Y.N., Makarov, M.I., 2017. Organochlorine compounds and the biogeochemical cycle of chlorine in soils: a review. Euras. Soil Sci. 50, 1025-1032. https://doi.org/10.1134/S1064229317090113

Wakatsuki, T., Rasyidin, A., 1992. Rates of weathering and soil formation. Geoderma 52, 251-263. https://doi.org/10.1016/0016-7061(92)90040-E

Wilson, M.J., 1987. X-ray powder diffraction methods, in: Wilson, M.J. (Ed.), A Handbook of Determinative Methods in Clay Mineralogy. Chapman & Hall, New York, pp. 26-98.

Yoo, K., Amundson, R., Heimsath, A.M., Dietrich, W.E., Brimhall, G.H., 2007. Integration of geochemical mass balance with sediment transport to calculate rates of soil chemical weathering and transport on hillslopes. J. Geophys. Res. 112, F02013. https://doi.org/10.1029/2005JF000402

Bullet points

- Geochemical modelling made it possible quantifying rates of pedogenic processes
- Soil formation rates on the Pantanal ridges range from 396 to 638 kg ha^{-1} y^{-1}
- It takes at least 125 y to generate the Pantanal alkaline lakes
- Downslope soils act as a buffer that preserves lake alkalinity
- Deep pH 3.5 horizon due to mixing of alkaline and acid groundwater

Supplementary material

Table A.1 – Values related to Fig. 6. Number of moles precipitated (positive values) or dissolved (negative values) minerals corresponding to the formation of 1 L of deep groundwater. Ef: evaporation factor; Anort: anortite; Alb: albite, Musc: muscovite; K-Feld: K-Feldspar; Goe: goethite; Ill: Illite; Am-SiO_2: amorphous silica; Fe-Kaol: ferriferous kaolinite; Fe-Beid: ferribeidellite.

Model solution l	Ef	Minerals								
		Dissolution (mol)						Precipitation (mol)		
		Anort	Alb	Musc	K-Feld	Goe	Ill	Am-SiO_2	Fe-Kaol	Fe-Beid
a	0.56	$-4.5\ 10^{-5}$	$-9.3\ 10^{-5}$		$-1.2\ 10^{-4}$	$-2.1\ 10^{-5}$	$-4.0\ 10^{-5}$	$4.4\ 10^{-4}$	$2.1\ 10^{-4}$	
b	0.56	$-4.5\ 10^{-5}$	$-9.3\ 10^{-5}$	$-1.2\ 10^{-4}$		$-2.1\ 10^{-5}$	$-4.0\ 10^{-5}$	$1.9\ 10^{-5}$	$3.4\ 10^{-4}$	
c	0.56	$-5.7\ 10^{-5}$	$-9.3\ 10^{-5}$		$-6.9\ 10^{-5}$	$-1.1\ 10^{-4}$	$-1.5\ 10^{-4}$	$3.2\ 10^{-4}$		$2.5\ 10^{-4}$
d	0.56	$-6.8\ 10^{-5}$	$-9.3\ 10^{-5}$	$-5.4\ 10^{-5}$		$-1.4\ 10^{-4}$	$-1.8\ 10^{-4}$	$1.8\ 10^{-4}$		$3.1\ 10^{-4}$

Table A.2 – Values related to Fig. 7. Number of moles of precipitated minerals corresponding to the evaporation of 10 L of an average alkaline lake water. SiO_2 am: amorphous SiO_2.

Precipitated	% of evaporation													
mineral	10	80	90	91	92	93	94	95	96	97	98	99	99,91	99,96
Calcite	$6,5\ 10^{-3}$	$6,6\ 10^{-3}$	$6,6\ 10^{-3}$	$6,6\ 10^{-3}$	$6,6\ 10^{-3}$	$6,6\ 10^{-3}$	$6,6\ 10^{-3}$	$6,6\ 10^{-3}$	0	0	0	0	0	0
Dolomite	$1,6\ 10^{-3}$	$1,6\ 10^{-3}$	$1,6\ 10^{-3}$	$1,6\ 10^{-3}$	$1,6\ 10^{-3}$	$1,6\ 10^{-3}$	$1,6\ 10^{-3}$	$1,6\ 10^{-3}$	$1,6\ 10^{-3}$	$1,6\ 10^{-3}$	$1,6\ 10^{-3}$	$1,6\ 10^{-3}$	$1,6\ 10^{-3}$	$1,6\ 10^{-3}$
Gaylussite	0	0	0	0	0	0	0	0	$6,6\ 10^{-3}$	0	0	0	0	0
Glaserite	0	0	0	0	0	0	0	0	0	0	0	0	0	$2,3\ 10^{-3}$
Halite	0	0	0	0	0	0	0	0	0	0	0	0	0	$3,5\ 10^{-1}$
Nahcolite	0	0	0	0	0	0	0	0	0	0	0	0	$8,9\ 10^{-1}$	$9,3\ 10^{-1}$
Pirssonite	0	0	0	0	0	0	0	0	0	$6,6\ 10^{-3}$	$6,6\ 10^{-3}$	$6,6\ 10^{-3}$	$6,6\ 10^{-3}$	$6,6\ 10^{-3}$
SiO2 am	$9,9\ 10^{-1}$	$9,8\ 10^{-1}$	$9,6\ 10^{-1}$	$9,5\ 10^{-1}$	$9,5\ 10^{-1}$	$9,4\ 10^{-1}$	$9,3\ 10^{-1}$	$9,2\ 10^{-1}$	$9,1\ 10^{-1}$	$9,0\ 10^{-1}$	$8,8\ 10^{-1}$	$8,9\ 10^{-1}$	1,0	$5,0\ 10^{-5}$
Sylvite	0	0	0	0	0	0	0	0	0	0	0	0	2,2	$2,4\ 10^{-1}$

Table A.3 – Values related to Fig. 8. Number of moles of precipitated (positive values) or dissolved (negative values) minerals corresponding to the formation of 1 L of green sandy-loam groundwater. SiO_2 am: amorphous SiO_2; Fe-Beid: ferribeidellite; Fe-Kaol: ferriferous kaolinite.

Model solution number	Goethite	Quartz or SiO_2 am	Fe-Beid	Stevensite	Fe-Kaol	Fe-Illite	Calcite	Dolomite	Nahcolite	Gypsum	Alum-K
1	$-1.4\ 10^{-1}$	$-3.0\ 10^{-1}$	$-2.4\ 10^{-1}$	$1.4\ 10^{-2}$	$2.37\ 10^{-1}$	$1.6\ 10^{-1}$	$1.5\ 10^{-2}$	$6.1\ 10^{-3}$	$3.3\ 10^{-3}$	$1.3\ 10^{-4}$	0
2	$-1.2\ 10^{-1}$	$-2.0\ 10^{-1}$	$-2.4\ 10^{-2}$	$1.3\ 10^{-3}$	$-1.5\ 10^{-2}$	$8.8\ 10^{-2}$	0	0	$5.8\ 10^{-3}$	$1.3\ 10^{-4}$	0
3	$-1.3\ 10^{-1}$	$-2.4\ 10^{-1}$	$-7.0\ 10^{-2}$	$3.2\ 10^{-3}$	$3.3\ 10^{-2}$	$1.1\ 10^{-1}$	$2.8\ 10^{-3}$	0	$3.0\ 10^{-3}$	$1.3\ 10^{-4}$	0
4	$-1.5\ 10^{-1}$	$-2.1\ 10^{-1}$	$-3.7\ 10^{-2}$	0	$-1.2\ 10^{-2}$	$1.1\ 10^{-1}$	$-1.9\ 10^{-3}$	$3.8\ 10^{-3}$	0	0	$6.5\ 10^{-5}$
5	$-4.4\ 10^{-2}$	0	0	$3.2\ 10^{-3}$	$-1.7\ 10^{-2}$	$3.1\ 10^{-2}$	$7.0\ 10^{-3}$	$-7.6\ 10^{-3}$	$1.4\ 10^{-2}$	0	$6.5\ 10^{-5}$
6	$-1.3\ 10^{-1}$	$-2.3\ 10^{-1}$	$-3.3\ 10^{-2}$	$8.4\ 10^{-4}$	$-1.1\ 10^{-2}$	$1.0\ 10^{-1}$	0	$1.4\ 10^{-3}$	$3.0\ 10^{-3}$	$1.3\ 10^{-4}$	0
7	$-1.3\ 10^{-1}$	$-2.4\ 10^{-1}$	$-6.7\ 10^{-2}$	$3.1\ 10^{-3}$	$2.9\ 10^{-2}$	$1.1\ 10^{-1}$	$2.8\ 10^{-3}$	0	$3.0\ 10^{-3}$	0	$6.5\ 10^{-5}$
8	$-1.2\ 10^{-1}$	$-2.1\ 10^{-1}$	$-3.9\ 10^{-2}$	$1.8\ 10^{-3}$	0	$9.7\ 10^{-2}$	$1.5\ 10^{-3}$	0	$4.2\ 10^{-3}$	$1.3\ 10^{-4}$	0
9	$-1.2\ 10^{-1}$	$-2.1\ 10^{-1}$	$-3.9\ 10^{-2}$	$1.8\ 10^{-3}$	0	$9.7\ 10^{-2}$	$1.7\ 10^{-3}$	0	$4.1\ 10^{-3}$	0	$6.5\ 10^{-5}$
10	$-1.7\ 10^{-1}$	$-3.5\ 10^{-1}$	$-2.5\ 10^{-1}$	$1.3\ 10^{-2}$	$2.3\ 10^{-1}$	$1.8\ 10^{-1}$	$1.3\ 10^{-2}$	$-3.5\ 10^{-3}$	0	$1.3\ 10^{-4}$	0

Table A.4. – Values related to Fig. 9. Values corresponding to 1 L of mixture. DG: deep groundwater; ADHG: alkaline deep horizons groundwater; ALW: alkaline lake water; Am-SiO_2: amorphous silica.

Solution mixture	pH	Mineral precipitation (mol)					
		Calcite	Dolomite	Goethite	Am-SiO_2	Kaolinite	Stevensite
0.5 L DG + 0.5 L ADHG	3.2	$2.4\ 10^{-4}$	$2.3\ 10^{-4}$	$2.2\ 10^{-4}$	$2.0\ 10^{-2}$	0	$2.0\ 10^{-6}$
0.72 L DG + 0.28 L ALW	3.5	$2.5\ 10^{-4}$	0	$4.4\ 10^{-5}$	$2.0\ 10^{-2}$	$5.1\ 10^{-7}$	$2.6\ 10^{-5}$
0.64 L DG + 0.18 L ADHG + 0.18 L ALW	3.3	$2.8\ 10^{-4}$	$6.4\ 10^{-5}$	$1.0\ 10^{-4}$	$2.2\ 10^{-2}$	0	$2.6\ 10^{-5}$